Materials Science & Engineering A 820 (2021) 141504

Contents lists available at ScienceDirect

Materials Science & Engineering A

journal homepage: www.elsevier.com/locate/msea

# Grain size effect on tensile deformation behaviors of pure aluminum

B.B. Wang [a,c], G.M. Xie [b], L.H. Wu [c], P. Xue [c,*], D.R. Ni [c], B.L. Xiao [c], Y.D. Liu [a], Z.Y. Ma [c]

[a] School of Materials Science and Engineering, Northeastern University, 3-11 Wenhua Road, Shenyang, 110819, China
[b] State Key Laboratory of Rolling and Automation, Northeastern University, 3-11 Wenhua Road, Shenyang, 110819, China
[c] Shi-changxu Innovation Center for Advanced Materials, Institute of Metal Research, Chinese Academy of Sciences, 72 Wenhua Road, Shenyang, 110016, China

ARTICLE INFO

*Keywords:*
Grain size effect
Tensile properties
Hall-petch relationship
Strengthening mechanism

ABSTRACT

Grain refinement is a very effective method to improve the mechanical properties of materials and attracts widespread interests among researchers. However, the grain size effect on the mechanical properties is still unclear due to the undesirable microstructure in ultrafine grained (UFG) materials. In the present work, series of ideal materials with average grain sizes range from 0.7 μm to 30.0 μm containing high fraction of high angle grain boundaries (HAGBs), equiaxed grains and low density of dislocations were produced by friction stir processing (FSP). It was found that the Hall-Petch relationships could be classified into three stages as the grain size reduced from coarse grain to UFG regimes, which were decided by the strengthening mechanisms during tensile deformation. The strengthening effect of HAGBs (71 MPa·$\mu m^{1/2}$) was almost three times of low angle grain boundaries (25 MPa·$\mu m^{1/2}$), resulting in the positive deviation of Hall-Petch slope in fine grain regime by the increased specific surface area of HAGBs. The further positive deviation of the Hall-Petch slope in UFG regime was affected by the occurrence of an extra dislocation source limited strengthening mechanism, which was up to 29 MPa and reached to about 20% of the yield strength. The increased recovery rate of dislocations at HAGBs contributed to the decrease of mobile dislocation density, leading to the losing of work hardening in UFG regime during tensile deformation.

## 1. Introduction

As well-known, grain refinement is a very effective method to improve the mechanical properties. Therefore, nanostructured and ultrafine-grained (UFG) materials have attracted widespread interests among researchers due to the presence of large amount of grain boundaries in the materials contributing to the excellent mechanical properties [1–6]. The contribution of grain refinement to the improved yield strength (YS) can be elucidated by the well-known Hall-Petch relationship in conventional coarse grain (CG) and fine grain (FG) regimes [7,8]. However, as the grain size decreased to UFG regime, traditional work hardening mechanism would not work, as the comparable size between the ultrafine grains with the elementary unit of the dislocation structures formed during tensile deformation process. Therefore, the relationship between grain size and tensile strength of UFG material should be different from that of CG and FG materials. Although, the deviation phenomenon of Hall-Petch slope in UFG range has been reported in various studies, no consensus conclusion has been reached [9–12].

Nowadays, various severe plastic deformation (SPD) technologies, such as equal channel angle pressing (ECAP), high-pressure torsion (HPT), accumulative roll bonding (ARB), have become the main methods to prepare bulk UFG materials [13,14,16–18]. However, the materials usually exhibit elongated grains, high density of dislocations and high fraction of low-angle boundaries (LAGBs) [19–30]. Besides the grain size, grain aspect ratio (GAR), dislocation density, and grain boundary characteristics will significantly affect the tensile properties [31–33]. In order to investigate the grain size effect on the tensile deformation behaviors, a series of model materials with uniform equiaxed grains, low dislocation density, high fraction of high angle grain boundaries (HAGBs, misorientation angle $\geq 15°$) and weak texture are required. Although researchers kept trying to avoid or minimize the microstructural variation in different grain size regimes, the results were not so satisfactory [19]. Therefore, preparing nearly ideal model materials with different grain sizes is still a difficult task.

Friction stir processing (FSP) is a new thermo-mechanical processing technology, which is invented, based on friction stir welding [34]. It has been proved that FSP is able to prepare CG, FG and UFG materials with different grain sizes by adjusting the processing parameters [35–37]. More importantly, the grain refinement mechanism during FSP is

* Corresponding author.
*E-mail address:* pxue@imr.ac.cn (P. Xue).

https://doi.org/10.1016/j.msea.2021.141504
Received 1 January 2021; Received in revised form 27 March 2021; Accepted 5 May 2021
Available online 4 June 2021

dynamic recrystallization (DRX), which can avoid the high density of dislocations and strong shear textures, and uniform equiaxed grains with high fraction of HAGBs were usually obtained in the processed zone (PZ) [38]. Therefore, compared to the SPD methods, FSP provides an effective solution to prepare materials with different grain sizes and to investigate the grain size effect on the tensile properties.

In the present work, pure Al samples with various grain sizes were prepared by FSP under different parameters. We will focus on the transition of tensile deformation behavior and Hall-Petch relationship as the grain size reduced from the CG to UFG regimes, and the strengthening mechanisms will be discussed in detail.

## 2. Experiment methods

Commercially pure Al (1060) was used as the base material (BM). The plates were processed by FSP along the rolling direction, using a tool with a concave shoulder 12 mm in diameter and a conical threaded pin 4 mm in root diameter and the processing parameters are shown in Table 1. By adjusting the FSP parameters, samples with various average grain sizes ($d$) of 30 μm, 4.6 μm, 3.2 μm, 1.4 μm, 1.2 μm, 0.9 μm, 0.8 μm, and 0.7 μm were successfully obtained, which were measured from the electron back-scattered diffraction (EBSD) data including more than 300 grains and defined as CG-30, FG-4.6, FG-3.2, FG-1.4, FG-1.2, UFG-0.9, UFG-0.8, and UFG-0.7 samples, respectively.

The specimens for microstructural examinations were machined perpendicular to the FSP direction, as shown in Fig. 1. Microstructural characterization and analysis were carried out using optical microscopy (OM), scanning electron microscopy (SEM) and transmission electron microscopy (TEM). The specimens for OM observation were ground, polished, and then etched in a solution of 10 g NaOH and 100 ml $H_2O$ for about 2 min. TEM foils and EBSD samples were prepared by double-jet electrolytic polishing using a solution of 30 ml $HNO_3$ and 70 ml $CH_3OH$ at 248 K under a potential of 12 V. Tensile specimens, with a gauge length of 10 mm, width of 3 mm, and thickness of 2 mm, were machined in the center of the PZ parallel to the FSP direction (Fig. 1). Uniaxial tensile tests were carried out at room temperature with an initial strain rate of $1 \times 10^{-3}$ $s^{-1}$.

## 3. Results

### 3.1. Microstructure

It is observed from Fig. 1 that a basin-shaped PZ without defect and onion ring structure was obtained in the cross section perpendicular to the processing direction. The microstructural features were characterized by EBSD, and the images of some typical samples were shown in Fig. 2. The black lines and the white lines represent the HAGBs and LAGBs, respectively. All of the FSP samples exhibited uniform equiaxed grains with high fraction of HAGBs, indicating the occurrence of DRX in the PZs during FSP processing.

As exhibited in Fig. 3, the distributions of grain boundary misorientation angles in all FSP samples, irrespective of grain sizes, were similar to that of the random distribution for a cubic polycrystalline, while all FSP samples contained a large fraction of HAGBs (>70%). Huang et al. [39] studied the strengthening mechanisms in nanostructured and UFG materials, and indicated that the grain boundary misorientation angle significantly affected the yield stress. Apparently, FSP samples show similar distribution of misorientation angle as decreasing the grain size, which can exclude the influence of grain boundary characteristic on the mechanical properties.

Typical distribution of GARs for UFG-0.7 sample was shown in Fig. 4a. Only 5% of the GARs were larger than 2, and 68% of the GARs were less than 1.5. The average GAR value was equal to 1.5 for UFG-0.7 sample, and the distribution of the GAR was consistent with the normal distribution. The relationship between GAR distributions and grain sizes is shown in Fig. 4b. As decreasing the grain size, all samples exhibited similar distribution characteristics. It was clear that 60%–70% of the GARs were less than 1.5, and only 8% of the GARs were larger than 2 for all FSP samples. Tsuji et al. [15] reported that the average grain size of UFG Al fabricated by ARB was 270 nm, but the grains were elongated with the length as large as 1.2 μm at the long axis direction. The average GAR value was as high as 4.4 for the UFG Al prepared by this monotonic deformation method. Meanwhile, GAR significantly affected the accuracy of grain size measurement and the mechanical anisotropy, and further influenced the relationship between grain size and tensile properties [40–42]. The average value of GAR was equal to about 1.5 for all FSP samples with different grain sizes, implying that nearly equiaxed grains were achieved for all processing conditions.

The TEM images in Fig. 5 exhibited the typical microstructural features of the specimens with various grain sizes. It is clear that equiaxed grains were observed in all samples with different grain sizes. Most grain boundaries were sharp, clear, and relatively straight, which were consisted with the characteristics of the HAGBs [34,43], as illustrated by arrows in Fig. 5. The dislocation density in grain interior was very low for all samples, owning to the occurrence of dynamic recovery and DRX during FSP [34,44].

Based on the analysis of EBSD and TEM microstructures, pure Al samples with grain sizes vary from 30 μm to 0.7 μm, containing high fraction of HAGBs, similar GAR value and low dislocation density, were prepared by FSP under different parameters. Compared to SPD methods, FSP provides an effective solution to prepare nearly ideal model materials to investigate the real relationship between the grain size and the tensile properties from CG to UFG regimes.

### 3.2. Tensile properties

Fig. 6 shows the tensile stress-strain curves of FSP samples with various grain sizes, and the mechanical properties are listed in Table 1. As decreasing the grain size, the YS and ultimate tensile strength (UTS) gradually increased, and accompanied with the decrease of the uniform elongation and total elongation. CG-30 sample showed a typical continuous work hardening behavior with low YS of 43.6 MPa and high elongation of 59.5%. Compared with CG-30 sample, the curve of FG-1.2 sample exhibited a distinct yielding peak, and followed by a short stress platform region with greatly increased YS of 92.2 MPa and decreased elongation of 30.1%. As the grain size decreased to UFG regime, the curve of UFG-0.7 sample showed a distinct yielding peak followed by rapid strain softening with the highest YS of 142.5 MPa and the lowest

**Table 1**
Tensile properties and grain sizes of FSP samples under different processing parameters.

| Sample | Rotation rate (rpm) | Processing speed (mm/min) | Grain size (μm) | $w$ value (μm) | YS (MPa) | UTS (MPa) | $\sigma$(MPa) | Elongation (%) |
|---|---|---|---|---|---|---|---|---|
| CG-30 | 1500 | 100 | 30 | 1.21 | 43.6 ± 2.3 | 89.3 ± 2.4 | 124.0 ± 2.4 | 59.5 ± 1.1 |
| FG-4.6 | 800 | 100 | 4.6 | 1.30 | 59.8 ± 2.4 | 90.1 ± 2.0 | 115.2 ± 2.0 | 41.3 ± 0.7 |
| FG-3.2 | 800 | 400 | 3.2 | 1.35 | 67.4 ± 1.4 | 94.3 ± 1.8 | 110.7 ± 1.8 | 25.6 ± 0.4 |
| FG-1.4 | 800 | 800 | 1.4 | 1.23 | 85.0 ± 1.9 | 103.7 ± 1.2 | 121.7 ± 1.2 | 38.6 ± 1.3 |
| FG-1.2 | 600 | 800 | 1.2 | 1.25 | 92.2 ± 2.7 | 109.2 ± 2.6 | 119.5 ± 2.6 | 30.1 ± 0.5 |
| UFG-0.9 | 200 | 50 | 0.9 | 1.14 | 115.6 ± 2.1 | 125.2 ± 2.9 | 131.7 ± 2.9 | 28.5 ± 0.6 |
| UFG-0.8 | 400 | 800 | 0.8 | 0.96 | 130.0 ± 3.4 | 155.2 ± 3.7 | 155.8 ± 3.7 | 16.1 ± 0.4 |
| UFG-0.7 | 100 | 20 | 0.7 | 0.86 | 142.5 ± 2.3 | 172.8 ± 3.3 | 173.4 ± 3.3 | 11.3 ± 0.2 |

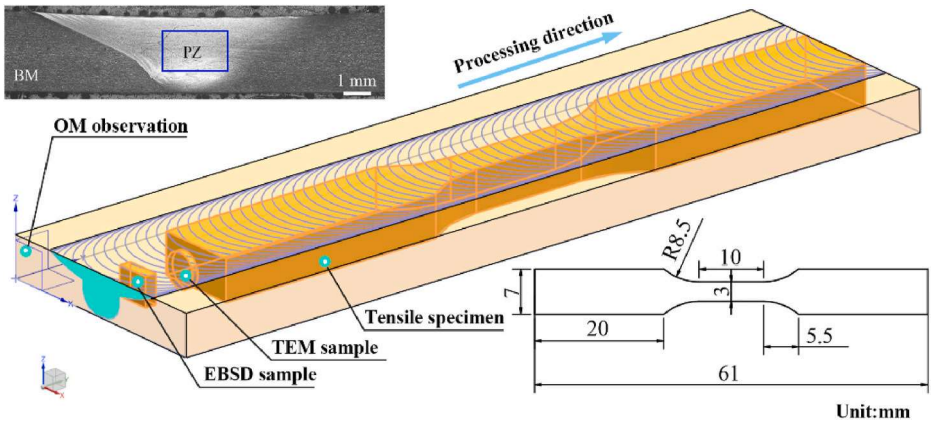


**Fig. 1.** Schematic illustration of FSP and the sample locations for tensile tests and microstructure observations.

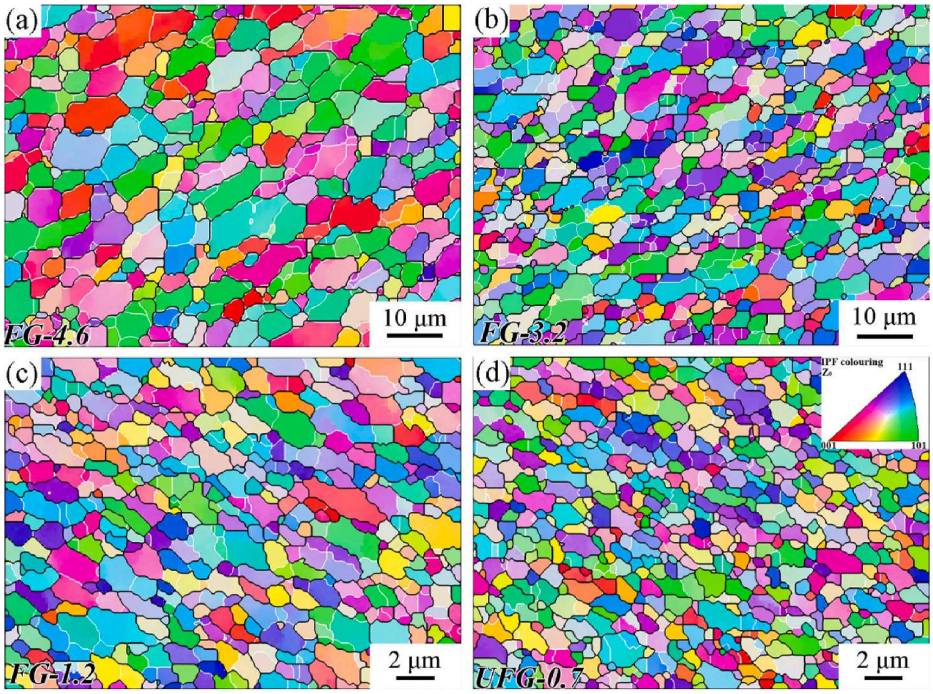


**Fig. 2.** EBSD images of samples with different grain sizes: (a) FG-4.6, (b) FG-3.2, (c) FG-1.2, (d) UFG-0.7.

elongation of 11.3%.

It is well known that the YS ($\sigma_y$) is related to the average grain size ($d$) by the classical Hall-Petch relationship:

$$\sigma_y = \sigma_0 + k \cdot d^{-1/2} \tag{1}$$

where $\sigma_0$ and $k$ represent the friction stress and the slope of Hall-Petch relationship, respectively. Fig. 7 shows the Hall-Petch relationship of pure Al specimens prepared by FSP in this study. The values of $\sigma_0$ and $k$ were 28 MPa and 67 MPa·μm$^{1/2}$ by fitting the data to equation (2) at CG and FG regimes, respectively. However, the fitting result of $k$ value at UFG regime was 396 MPa·μm$^{1/2}$, which was much higher than that of FG material.

## 4. Discussion

### 4.1. Tensile deformation behavior

According to the curve characteristics in Fig. 6, the tensile stress-strain curves can be classified into three different categories with the change of grain size:

Type I ($d > 1.2$ μm): the curve shows continuous work hardening behavior similar to that of the CG material.

Type II ($0.9 \leq d \leq 1.2$ μm): the curve exhibits a distinct yielding peak, and follows by a short stress platform region (dynamic equilibrium between strengthening and softening processes) before a continuous strain softening.

Type III ($d < 0.9$ μm): the curve shows a distinct yielding peak following by a rapid strain softening.

Previous studies indicated that rapid strain softening and attendant loss of ductility were the main tensile deformation characteristics as grain size decreased to UFG [45–47]. Strain hardening and softening phenomena were usually associated with the difference value between the steady state subgrain size and the actual grain size. A semi-empirical relationship between the shear stress, and the steady state subgrain size ($w$) has been well established, which can be expressed by the following equation [36,48–50]:

$$w = k_w b \frac{G}{\sigma} \tag{2}$$

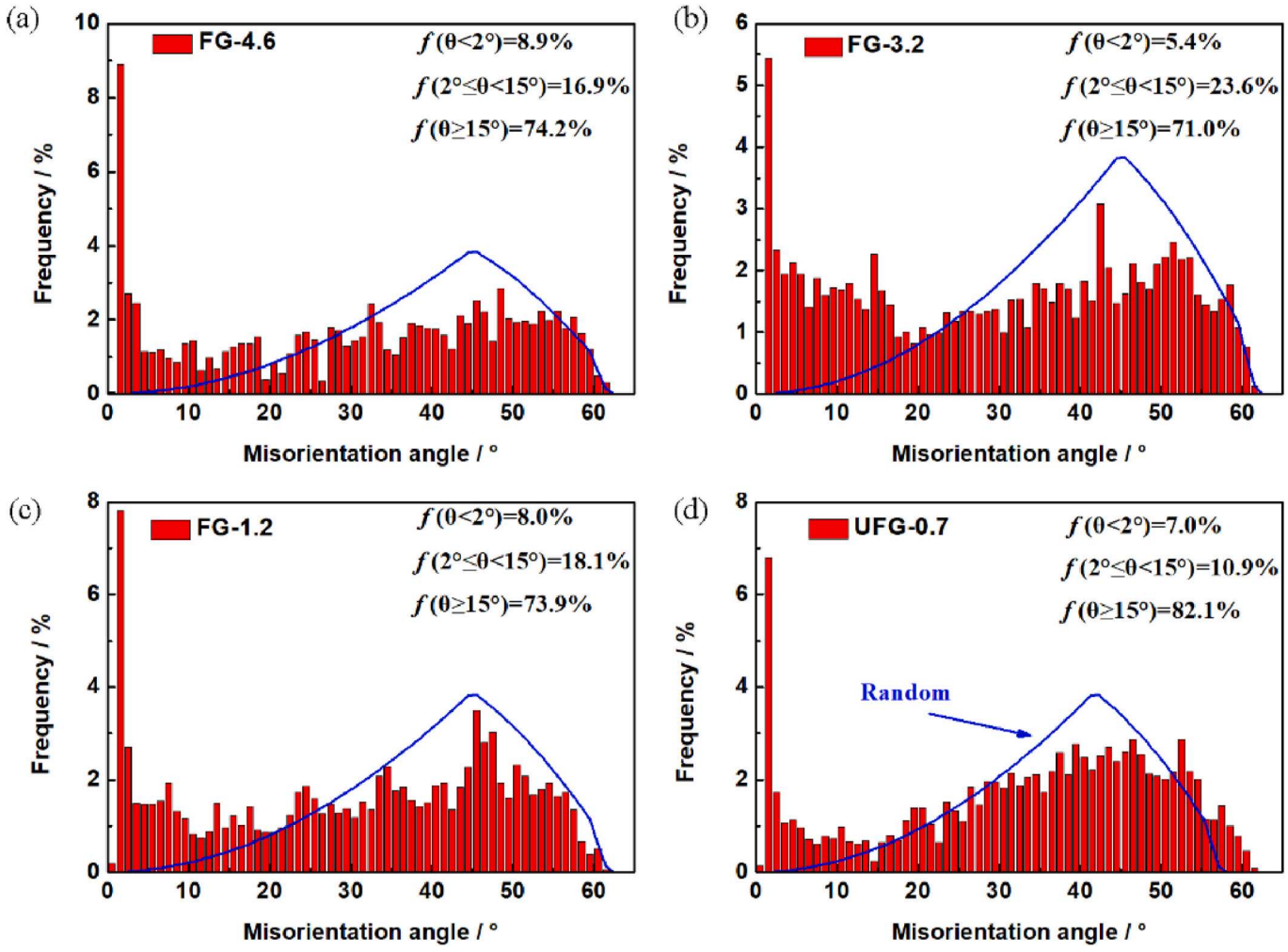


**Fig. 3.** Distributions of grain boundary misorientation angles of FSP samples: (a) FG-4.6, (b) FG-3.2, (c) FG-1.2, (d) UFG-0.7.

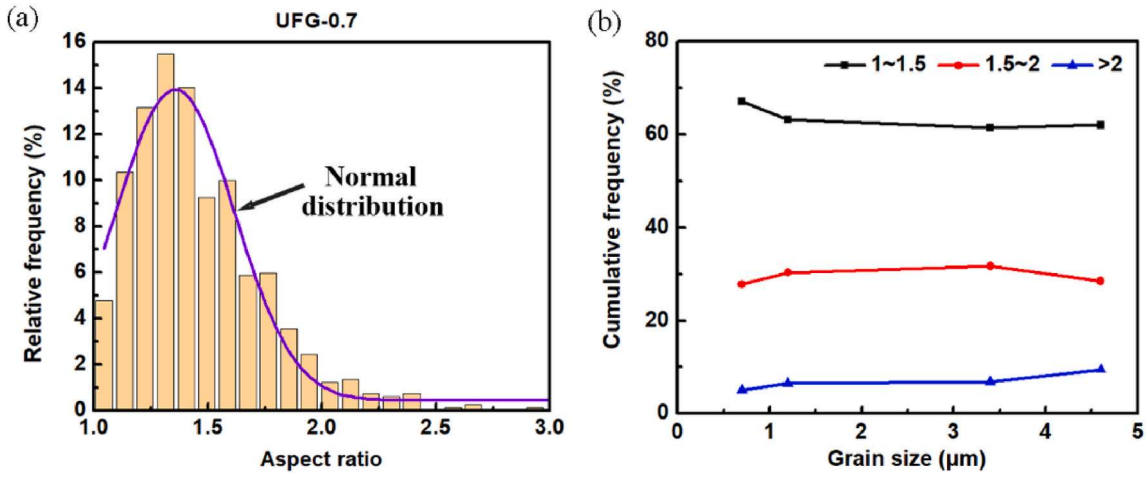


**Fig. 4.** (a) Typical distribution of GAR for UFG-0.7 sample, (b) the fraction of GAR of samples with various grain sizes.

where $G$ is shear modulus (26 GPa), $b$ is burgers vector (0.286 nm) and $\sigma$ is the maximum value of true stress listed in Table 1 $k_w$ is a constant value between 10 and 30, and the value of 20 was used in previous study [50]. $W$ value represents the minimum size of the dislocation sub-structure evolved during the tensile deformation process, and the calculated results are listed in Table 1. When the grain size was less than $w$ value, the stress field of grain boundary would hinder the formation of dislocation cell in grain interior.

The typical TEM microstructures of FG-4.6, FG-1.2, and UFG-0.7 samples after 2% tensile strain and final fracture are shown in Fig. 8. For FG-4.6 samples, some dislocation tangles could be observed in grain interior even with a small deformation of 2% tensile strain, as shown in

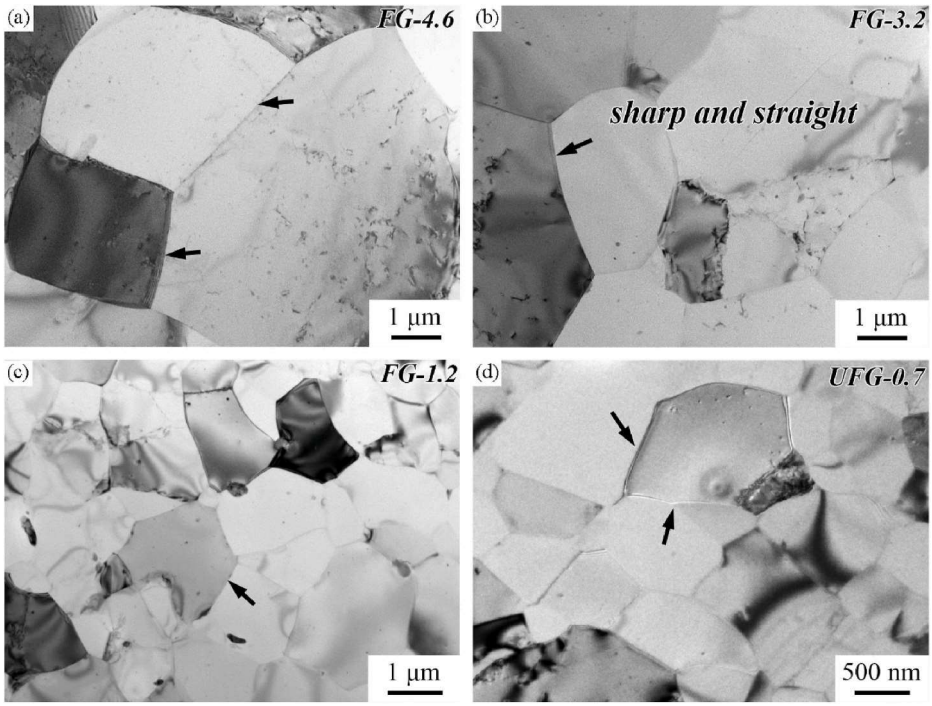


**Fig. 5.** Typical TEM microstructures of FSP pure Al samples: (a) FG-4.6, (b) FG-3.2, (c) FG-1.2, (d) UFG-0.7.

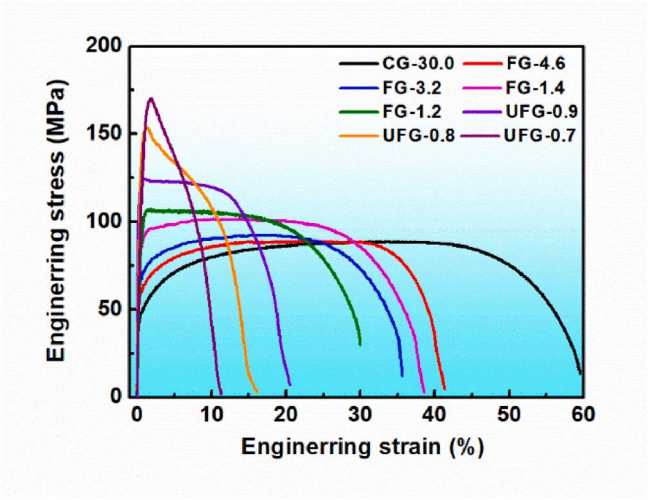


**Fig. 6.** Tensile engineering stress-strain curves of FSP samples with different grain sizes.

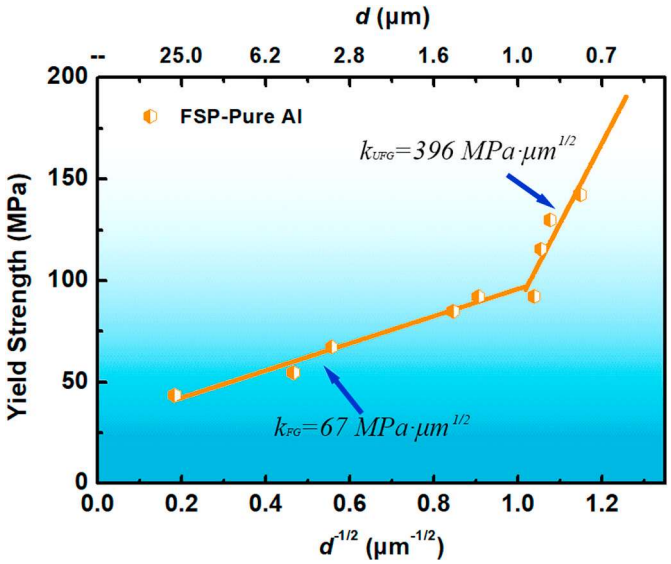


**Fig. 7.** Hall-Petch relationships of FSP pure Al samples.

Fig. 8a. Typical dislocation cell structures and a large amount of dislocation tangles formed in the grain interior after final fracture, as shown in Fig. 8d. The calculated *w* value was 1.30 μm for FG-4.6 sample, which was smaller than the grain size (4.6 μm). During the tensile test, the deformation promoted the nucleation and multiplication of dislocations in the grain interior for the CG and FG materials with Type I tensile stress-strain curves. With continued tensile deformation, dislocations multiplication and rearrangement resulted in the formation of dislocation cells in the grain interior, impeded the movement of dislocations, and enhanced the interactions between the dislocations. In this case, work hardening phenomenon occurred during the tensile deformation process for this type of materials.

Fig. 8b and e shows the TEM microstructures after 2% tensile strain and final fracture of FG-1.2 sample, respectively. Only a few dislocations could be observed in the grain interior after a small deformation of 2% tensile strain. Different from that of FG-4.6 sample, some dislocations began to accumulate near the grain boundaries, as shown by the arrows in Fig. 8b. Further, the final microstructure after fracture in FG-1.2 sample was obviously different from that of FG-4.6 sample. The distribution of dislocations was not uniform, resulting in tangled dislocations in some large grains and free of dislocation in some small grains. The calculated *w* value of FG-1.2 sample (1.25 μm) was almost equal to the average grain size (1.2 μm). In this case, the balance of the work hardening in the large grains ($d > w$) and strain softening in the small grains ($d < w$) contributed to a short steady state deformation for the Type II materials in tensile deformation.

Typical TEM microstructures of UFG-0.7 sample after 2% tensile strain and final fracture are exhibited in Fig. 8c and f, respectively. As the grain size decreased to UFG regime, the number of dislocations

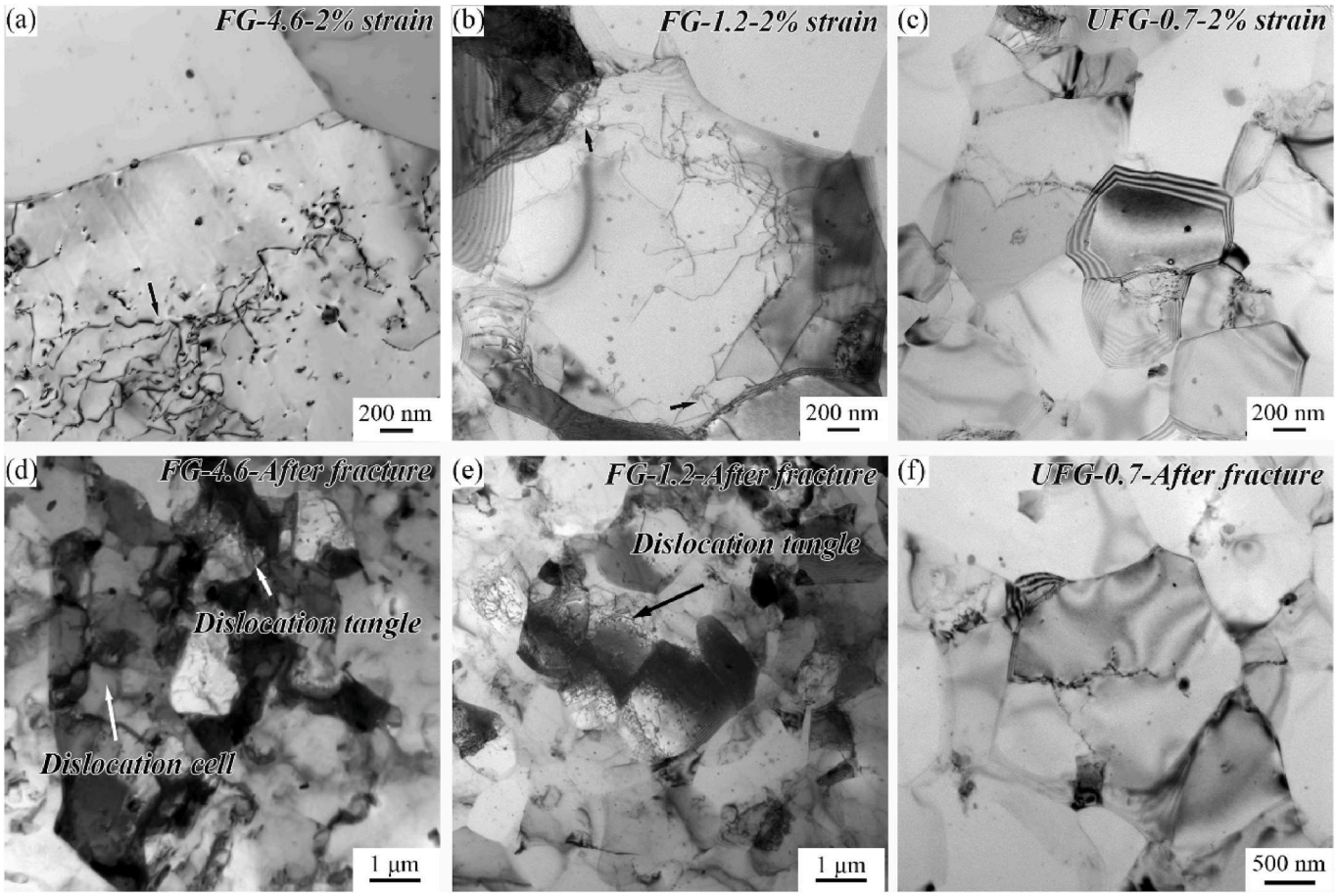


**Fig. 8.** TEM microstructures of FG-4.6, FG-1.2, UFG-0.7 samples after 2% tensile strain (a)–(c) and after final fracture (d)–(e).

decreased dramatically, few dislocations could be found even after final fracture. The calculated $w$ value of UFG-0.7 sample (0.86 μm) was larger than the grain size (0.7 μm), so the dislocation substructures were hard to form in the grain interior due to the rapid recovery at the grain boundary. Therefore, only a few dislocations piled up at the grain boundary, and most of the grains were free of dislocation, which was consisted with the strain softening performance and poor dislocation storage ability [51].

### 4.2. Hall-Petch relationship

To make the comparison of Hall-Petch relationship more impartial, materials prepared by FSP and SPD methods were compared in this study [27,51–53]. The purity has an effect on the intercept of the Hall-Petch relationship [8,54]. Therefore, all data were normalized by making the intercept values consistent with the high purity Al to exclude the influence of material purity, and the results were shown in Fig. 9. Clearly, the Hall-Petch relationships can be divided into three stages. At the stage I ($d \geq 25$ μm), the primary barrier for dislocation glide was dominated by dislocation substructures during the tensile deformation process. The data points for CG materials followed the Hall-Petch relationship with a lower $k_I$ value between 25 and 41 MPa· $\mu m^{1/2}$ [27]. $k_I$ value can be affected by texture, dislocation density, and the fraction of HAGBs, so the range was relatively wide due to the various microstructures prepared by different methods. The YS in stage I can be written as the following equation:

$$\sigma_{I,\ d\geq 25\ \mu m} = \sigma_0 + k_I \cdot d^{-1/2} = 9.7 \quad + \quad (25 \sim 41) \quad \cdot d^{-1/2} \tag{3}$$

At the stage II (1 μm $\leq d <$ 25 μm), the $k_{II}$ value was between 60 and 70 MPa·$\mu m^{1/2}$, which was larger than that of stage I. The YS in stage II

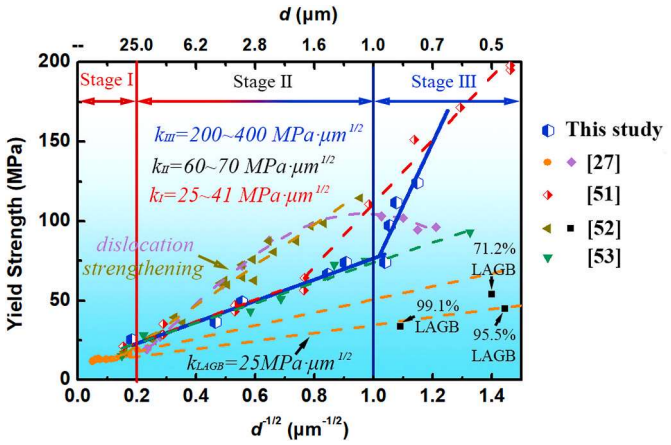


**Fig. 9.** Hall-Petch relationships of pure Al samples [27,51–53].

can be written as the following equation:

$$\sigma_{II,1\mu m\leq d<25\ \mu m} = \sigma_{FG} + k_{II} \cdot d^{-1/2} = 28 \quad + \quad (60 \sim 70) \quad \cdot d^{-1/2} \tag{4}$$

In this stage, the specific surface area of HAGBs was increased as the decrease of grain size. Therefore, dislocation tangled or assembled at the HAGBs brought stronger strengthening effect than the LAGBs and dislocation substructures, resulting in an increase of $k_{II}$ compared to $k_I$. Previous studies indicated that the dislocation strengthening was even larger than grain boundary strengthening due to high density of dislocations in the materials prepared by cold rolling and ARB methods, resulting in a higher Hall-Petch slope of 131 MPa·$\mu m^{1/2}$ [52] in stage II,

as illustrated by arrows in Fig. 9. On the contrary, the dislocation density of FSP material was very low attributed to the DRX process.

At the stage III ($d < 1$ μm), the $k_{III}$ value was between 200 and 400 MPa·μm$^{1/2}$ in UFG regime, which was significantly higher than CG and FG materials. The microstructural differences were very large for different UFG materials due to the different deformation degree during SPD processes, and a high fraction of non-equilibrium grain boundaries were usually obtained. Therefore, the deviation of the actual grain size was very big, resulting in a big range of $k_{III}$ value. The YS in stage III can be written as the following equation:

$$\sigma_{III,\ d<1\mu m} = \sigma_{UFG} + k_{III} \cdot d^{-1/2} = -307 \quad + \quad (200 \sim 400) \quad \cdot \mathrm{d}^{-1/2} \tag{5}$$

In equation (5), the intercept value ($\sigma_{UFG}$) didn't represent the lattice friction stress, which contained the lattice friction stress and other strengthening mechanisms, and a negative intercept value (−307 MPa) was suited for the Hall-Petch relationship in stage III. Yu et al. [51] had reported that the fitting result of $k$ value for ECAP UFG material was much higher than that of FG material, and the initial inhomogeneous flow resulted in the positive deviation of the Hall–Petch relationship in the UFG regime. Meanwhile, the dislocation densities of UFG materials produced by ECAP and ARB were higher than the FG materials prepared by combination of SPD and following annealing processes, which would contribute higher dislocation strengthening in SPD UFG material than that in FG material. However, no obvious inhomogeneous flow was observed in UFG-0.7 sample. Furthermore, the dislocation density of FSP UFG material was similar to that of FG material and kept a relatively low value. Therefore, the $k_{III}$ value of FSP UFG materials was much higher than $k_{II}$ and $k_I$, and even higher than that of ECAP UFG material. This was not be affected by the inhomogeneous flow and increased dislocation density, so an extra strengthening mechanism should play a more important role.

### 4.3. Strengthening mechanisms

Some models have been proposed to explain the Hall-Petch relationship and give expression for $k$ value [54]. In these models, the $k$ value was decided by dislocation density, GAR, and grain boundary characteristics, which were related to the strengthening mechanism of materials.

The strengthening mechanism of CG and FG materials mainly contained the grain boundary strengthening and dislocation strengthening ($\sigma_{dis}$). Most of the dislocations stored in grain interior and LAGBs. Previous research indicated that the LAGBs with misorientation angle below 2° acted as dislocation strengthening and the rest of the grain boundaries were regarded as grain boundary strengthening [52]. Based on this assumption, the YS can be written in the following way:

$$\sigma_{YS} = \sigma_0 + \sigma_{dis} + \sigma_{GB} \tag{6}$$

where $\sigma_{dis}$ represents the dislocation strengthening, and $\sigma_{GB}$ is grain boundary strengthening. $\sigma_{dis}$ can be written as:

$$\sigma_{dis} = M\alpha Gb\sqrt{\rho_0 + \frac{3(1 - f_{\theta\geq 2^\circ})\theta_{ave,<2^\circ}}{bd}} \tag{7}$$

where $f_{\theta\geq 2^\circ}$ represents the fraction of grain boundaries with misorientation angles above 2°, $\theta_{ave,<2^\circ}$ is the average value of misorientation angle below 2°, $M$ is the Taylor factor (3.06), $\alpha$ is a constant (0.24), $G$ is the shear modulus (26 GPa), $b$ is the burgers vector (0.286 nm), $\rho_0$ is dislocation density in grain interior [27,52]. The dislocations mainly stored in the LAGBs with misorientation angle below 2°, and the dislocation density in grain interior ($\rho_0$) was relatively small due to the DRX during FSP, which can be ignored in this study.

Previous research indicated that grain boundary characteristic had a strong effect on the tensile deformation behavior [55]. Most of the previous literatures only focused on the grain size effect on the Hall-Petch relationship, but ignored the influence of grain boundary characteristics [56,57]. However, the strengthening effect was different between LAGBs and HAGBs, leading to a strong influence on the relationship of grain size and tensile properties. Therefore, grain boundary strengthening divides into LAGBs strengthening and HAGBs strengthening, which can be written as:

$$\sigma_{GB} = \sigma_{LAGB} + \sigma_{HAGB} = k_{LAGB}\sqrt{\frac{f_{2^\circ\leq\theta<15^\circ}}{d}} + k_{HAGB}\sqrt{\frac{f_{\theta\geq 15^\circ}}{d}} \tag{8}$$

where $k_{LAGB}$ is the Hall-Petch slope for LAGBs strengthening, $k_{HAGB}$ is the Hall-Petch slope for HAGBs strengthening. The $k_{LAGB}$ can be obtained at the situation where the LAGB dominated the grain boundary strengthening for the CG materials at the stage I. $k_{LAGB}$ was equal to 25 MPa·μm$^{1/2}$, which was the minimize value of $k_I$ through fitting the Hall-Petch relationship of LAGBs, as shown in Fig. 9. $\sigma_{HAGB}$ and $k_{HAGB}$ can be calculated by the following equations:

$$\sigma_{HAGB} = \sigma_{YS} - \sigma_0 - \sigma_{dis} - \sigma_{LAGB} \tag{9}$$

$$k_{HAGB} = \sigma_{HAGB} \Big/ \sqrt{\frac{f_{\theta\geq 15^\circ}}{d}} \tag{10}$$

The values of $\sigma_{HAGB}$ and $k_{HAGB}$ of the FG-4.6 and FG-3.2 samples were calculated through equation (9) and (10), as shown in Table 2. The $k_{HAGB}$ value, representing the HAGBs strengthening for pure Al with any grain size, can be defined as the average value of those of the FG-4.6 and FG-3.2 samples, which was equal to 71 MPa·μm$^{1/2}$. In order to verify the accuracy of the above results, $k_{LAGB}$ and $k_{HAGB}$ were used to calculate the YS of FG-1.2 sample. The calculated YS of FG-1.2 sample was 95.5 MPa, which was nearly equal to the actual result (92.2 MPa), proving the accuracy of $k_{lAGB}$ and $k_{HAGB}$ values. Obviously, the $k_{HAGB}$ value (71 MPa·μm$^{1/2}$) is almost three times of $k_{lAGB}$ (25 MPa·μm$^{1/2}$), meaning that the HAGBs are more efficient than LAGBs in material strengthening, which resulted in a higher Hall-Petch slope in stage.

When the grain size decreases to UFG regime (stage III), the grain refinement increased the probability of dislocation sinking at the HAGBs. The increased recovery rate of dislocations near the grain boundaries led to the decrease of mobile dislocation density. Previous studies have proposed that significantly reduced dislocation source density resulted in an additional strengthening mechanism and a higher stress for UFG or nanostructured materials by activating alternative dislocation source [27]. Huang et al. [39,58] found that the YS of UFG material could be increased by annealing, because the generation and interaction of dislocations reduced under heat treatment, leading to an increase in YS in order to activate new dislocation sources during tensile deformation. Kamikawa et al. [27] called this strengthening mechanism as dislocation source limited strengthening, which usually appeared in UFG and nanostructure materials where dislocations were significantly reduced. The dislocation source limited strengthening ($\sigma_{source}$) in UFG-0.7 sample can be acquired by the following equation:

$$\sigma_{source} = \sigma_{YS,\ UFG-0.7} - \sigma_0 - \sigma_{dis} - \sigma_{LAGB} - \sigma_{HAGB} \tag{11}$$

The $\sigma_{source}$ value of UFG-0.7 sample was calculated as 29 MPa according to equation (11), which reached to about 20% of the YS of UFG-0.7 sample.

Fig. 10 shows the distribution of different strengthening mechanisms contributed to the YS of some typical samples. Strengthening mechanisms of FG materials mainly included dislocation strengthening and HAGBs strengthening. The contribution of LAGBs strengthening to YS was less than 10% for FG and UFG materials. Previous research indicated that the dislocation strengthening was larger than grain boundary strengthening due to the high density of dislocations stored in LAGBs with misorientation angle below 2° [52]. However, the dislocation strengthening of FSP sample was relatively weak due to the low fraction of LAGBs. The primary strengthening mechanisms of UFG materials were HAGBs strengthening and dislocation source limited strengthening

**Table 2**
Structural parameters for different strengthening mechanisms.

| Sample | $k_{LAGB}$ (MPa·μm$^{1/2}$) | LAGBs strengthening (MPa) | Dislocation strengthening (MPa) | $k_{HAGB}$ (MPa·μm$^{1/2}$) | HAGBs strengthening (MPa) |
|---|---|---|---|---|---|
| FG-4.6 | 25.00 | 4.75 | 22.13 | 70 | 23.22 |
| FG-3.2 | 25.00 | 6.75 | 17.23 | 72 | 33.72 |
| FG-1.2 | 25.00 | 9.62 | 24.51 | 71 | 55.28 |
| UFG-0.7 | 25.00 | 9.48 | 20.44 | 71 | 73.81 |

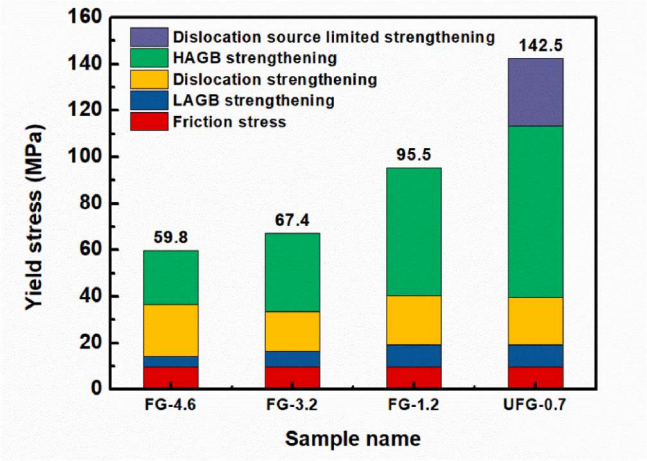


**Fig. 10.** The distributions of different strengthening mechanisms contribute to the YS.

which contributed a higher Hall-Petch slope in stage.

The calculation substantiates that the HAGBs strengthening increases with the decrease of grain size and acts as a dominant role in mechanical properties. The dislocation source limited strengthening reached to about 20% of the YS of UFG materials. Compared to FG material, the extra strengthening of UFG material, i.e. dislocation source limited strengthening, required higher stress to nucleate more mobile dislocations to maintain the plastic flow during tensile tests. Therefore, dislocation source limited strengthening contributed to higher YS, leading to the loss of work hardening during tensile tests.

## 5. Conclusions

Commercially pure Al (1060) samples with grain sizes range from 0.7 μm to 30.0 μm were produced by FSP with different processing parameters. Based on the experimental observations and discussions, the following conclusions can be obtained:

1. Irrespective of grain size, the grain morphology was equiaxed, and almost no dislocations were observed in grain interior. The distributions of grain boundary misorientation angles were similar to the random distribution and the fraction of the HAGBs was higher than 70%.
2. The Hall-Petch relationships were classified into three stages as the grain size reduced from CG to UFG regime. The strengthening effect of HAGBs was almost three times of LAGBs, resulting in the positive deviation of Hall-Petch slope in stage II. The further positive deviation of Hall-Petch relationship at UFG region was due to the occurrence of dislocation source limited strengthening.
3. The dislocation source limited strengthening reached to about 20% for the YS of UFG material, which resulted in the increased the YS and the decreased uniform elongation caused by the losing of work hardening during tensile deformation.

## Credit author statement

P. Xue and D.R. Ni led the project. B.B. Wang, G.M. Xie, L.H. Wu, D.R. Ni and B.L. Xiao designed and performed all of the experiments and analyzed the data including sample processing, property testing and microstructure characterization. B.B. Wang and P. Xue wrote the paper under the guidance of Y.D. Liu and Z.Y. Ma. All of the authors have discussed the results and revised the paper together.

## Data availability

The raw/processed data required to reproduce these findings cannot be shared at this time as the data also forms part of an ongoing study.

## Declaration of competing interest

The authors declare that they have no known competing financial interests or personal relationships that could have appeared to influence the work reported in this paper.

## Acknowledgements

This work was supported by the National Natural Science Foundation of China under grant No. 52071317, the Open Research Fund from the State Key Laboratory of Rolling and Automation, Northeastern University (2020RALKFKT009), and the Youth Innovation Promotion Association of the Chinese Academy of Sciences (2017236).

## References

[1] R.Z. Valiev, R.K. Islamgaliev, I.V. Alexandrov, Bulk nanostructured materials from severe plastic deformation, Prog. Mater. Sci. 45 (2000) 103–189.
[2] Y. Estrin, A. Vinogradov, Extreme grain refinement by severe plastic deformation: a wealth of challenging science, Acta Mater. 61 (2013) 782–817.
[3] X.H. An, S.D. Wu, Z.G. Wang, Z.F. Zhang, Significance of stacking fault energy in bulk nanostructured materials: insights from Cu and its binary alloys as model systems, Prog. Mater. Sci. 101 (2019) 1–45.
[4] T.G. Langdon, Twenty-five years of ultrafine-grained materials: achieving exceptional properties through grain refinement, Acta Mater. 61 (2013) 7035–7059.
[5] L.S. Toth, C. Gu, Ultrafine-grain metals by severe plastic deformation, Mater. Char. 92 (2014) 1–14.
[6] A. Azushima, R. Kopp, A. Korhonen, D.Y. Yang, F. Micari, G.D. Lahoti, P. Groche, J. Yanagimoto, N. Tsuji, A. Rosochowski, A. Yanagida, Severe plastic deformation (SPD) processes for metals, CIRP Ann 57 (2008) 716–735.
[7] H. Fujita, T. Tabata, Effect of grain-size and deformation substructure on mechanical properties of polycrystalline aluminum, Acta Metall. 21 (1973) 355–365.
[8] N. Hansen, The effect of grain size and strain on the tensile flow stress of aluminium at room temperature, Acta Metall. 25 (1977) 863–869.
[9] H.J. Choi, S.W. Lee, J.S. Park, D.H. Bae, Positive deviation from a Hall-Petch relation in nanocrystalline aluminum, Mater. Trans. 50 (2009) 640–643.
[10] W. Xu, L.P. Davila, Tensile nanomechanics and the Hall-Petch effect in nanocrystalline aluminium, Mater. Sci. Eng., A 710 (2018) 413–418.
[11] S.N. Naik, S.M. Walley, The Hall-Petch and inverse Hall-Petch relations and the hardness of nanocrystalline metals, J. Mater. Sci. 55 (2020) 2661–2681.
[12] B. Mirshekari, A. Zarei-Hanzaki, A. Barabi, H.R. Abedi, S.J. Lee, H. Fujii, An anomalous effect of grain refinement on yield stress in friction stir processed lightweight steel, Mater. Sci. Eng., A 799 (2021) 140057.
[13] A. Zhilyaev, T. Langdon, Using high-pressure torsion for metal processing: fundamentals and applications, Prog. Mater. Sci. 53 (2008) 893–979.
[14] H. Lanjewar, L.A.I. Kestens, P. Verleysen, Damage and strengthening mechanisms in severely deformed commercially pure aluminum: experiments and modeling, Mater. Sci. Eng., A 800 (2021) 140224.

[15] N. Tsuji, Y. Ito, Y. Saito, Y. Minamino, Strength and ductility of ultrafine grained aluminum and iron produced by ARB and annealing, Scripta Mater. 47 (2002) 893–899.
[16] Q. Liu, X. Huang, D.J. Lloyd, N. Hansen, Microstructure and strength of commercial purity aluminium (AA 1200) cold-rolled to large strains, Acta Mater. 50 (2002) 3789–3802.
[17] O.V. Mishin, D. Juul Jensen, N. Hansen, Microstructures and boundary populations in materials produced by equal channel angular extrusion, Mater. Sci. Eng., A 342 (2003) 320–328.
[18] T. Huang, L. Shuai, A. Wakeel, G. Wu, N. Hansen, X. Huang, Strengthening mechanisms and Hall-Petch stress of ultrafine grained Al-0.3%Cu, Acta Mater. 156 (2018) 369–378.
[19] M. Kawasaki, Z. Horita, T.G. Langdon, Microstructural evolution in high purity aluminum processed by ECAP, Mater. Sci. Eng., A 524 (2009) 143–150.
[20] M. Reihanian, R. Ebrahimi, N. Tsuji, M.M. Moshksar, Analysis of the mechanical properties and deformation behavior of nanostructured commercially pure Al processed by equal channel angular pressing (ECAP), Mater. Sci. Eng., A 473 (2008) 189–194.
[21] S. Qu, X.H. An, H.J. Yang, C.X. Huang, G. Yang, Q.S. Zang, Z.G. Wang, S.D. Wu, Z. F. Zhang, Microstructural evolution and mechanical properties of Cu-Al alloys subjected to equal channel angular pressing, Acta Mater. 57 (2009) 1586–1601.
[22] X.H. An, S.D. Wu, Z.G. Wang, Z.F. Zhang, Enhanced cyclic deformation responses of ultrafine-grained Cu and nanocrystalline Cu-Al alloys, Acta Mater. 74 (2014) 200–214.
[23] P. Bazarnik, Y. Huang, M. Lewandowska, T.G. Langdon, Structural impact on the Hall-Petch relationship in an Al-5Mg alloy processed by high-pressure torsion, Mater. Sci. Eng., A 626 (2015) 9–15.
[24] A. Loucif, R.B. Figueiredo, T. Baudin, F. Brisset, R. Chemam, T.G. Langdon, Ultrafine grains and the Hall-Petch relationship in an Al-Mg-Si alloy processed by high-pressure torsion, Mater. Sci. Eng., A 532 (2012) 139–145.
[25] X.H. An, Q.Y. Lin, S.D. Wu, Z.F. Zhang, R.B. Figueiredo, N. Gao, T.G. Langdon, Significance of stacking fault energy on microstructural evolution in Cu and Cu-Al alloys processed by high-pressure torsion, Philos. Mag. A 91 (2011) 3307–3326.
[26] R.W. Armstrong, 60 Years of Hall-petch: past to present nano-scale connections, Mater. Trans. 55 (2014) 2–12.
[27] N. Kamikawa, X. Huang, N. Tsuji, N. Hansen, Strengthening mechanisms in nanostructured high-purity aluminium deformed to high strain and annealed, Acta Mater. 57 (2009) 4198–4208.
[28] C.S. Pande, B.B. Rath, M.A. Imam, Effect of annealing twins on Hall-Petch relation in polycrystalline materials, Mater. Sci. Eng., A 367 (2004) 171–175.
[29] Y.Z. Tian, S. Gao, L.J. Zhao, S. Lu, R. Pippan, Z.F. Zhang, N. Tsuji, Remarkable transitions of yield behavior and Lüders deformation in pure Cu by changing grain sizes, Scripta Mater. 142 (2018) 88–91.
[30] X.H. An, S.D. Wu, Z.F. Zhang, R.B. Figueiredo, N. Gao, T.G. Langdon, Enhanced strength–ductility synergy in nanostructured Cu and Cu-Al alloys processed by high-pressure torsion and subsequent annealing, Scripta Mater. 66 (2012) 227–230.
[31] K. Matsumoto, T. Shibayanagi, Y. Umakoshi, Effect of grain-size on grain orientations and grain-boundary-character-distribution in recrystallized Al-0.3% Mg alloy, Scripta Metall. Mater. 33 (1995) 1321–1326.
[32] P.L. Sun, E.K. Cerreta, G.T. Gray III, J.F. Bingert, The effect of grain size, strain rate, and temperature on the mechanical behavior of commercial purity aluminum, Metall. Mater. Trans. 37 (2006) 2983–2994.
[33] M. Furukawa, Z. Horita, M. Nemoto, R.Z. Valiev, T.G. Langdon, Microhardness measurements and the Hall-Petch relationship in an Al-Mg alloy with submicrometer grain size, Acta Mater. 44 (1996) 4619–4629.
[34] R.S. Mishra, Z.Y. Ma, Friction stir welding and processing, Mater. Sci. Eng. R 50 (2005) 1–78.
[35] T. Hirata, T. Oguri, H. Hagino, T. Tanaka, S.W. Chung, Y. Takigawa, K. Higashi, Influence of friction stir welding parameters on grain size and formability in 5083 aluminum alloy, Mater. Sci. Eng., A 456 (2007) 344–349.
[36] S. Shukla, M. Komarasamy, R.S. Mishra, Grain size dependence of fatigue properties of friction stir processed ultrafine-grained Al-5024 alloy, Int. J. Fatig. 109 (2018) 1–9.
[37] H. Zhao, Q. Pan, Q. Qin, Y. Wu, X. Su, Effect of the processing parameters of friction stir processing on the microstructure and mechanical properties of 6063 aluminum alloy, Mater. Sci. Eng., A 751 (2019) 70–79.
[38] Y. Hu, H. Liu, S. Du, Achievement of high-strength 2219 aluminum alloy joint in a broad process window by ultrasonic enhanced friction stir welding, Mater. Sci. Eng., A (2020) 140587.
[39] X. Huang, N. Kamikawa, N. Hansen, Strengthening mechanisms in nanostructured aluminum, Mater. Sci. Eng., A 483–484 (2008) 102–104.
[40] A.B. Lopes, F. Barlat, J.J. Gracio, J.F.F. Duarte, E.F. Rauch, Effect of texture and microstructure on strain hardening anisotropy for aluminum deformed in uniaxial tension and simple shear, Int. J. Plast. 19 (2003) 1–22.
[41] D.J. Jensen, N. Hansen, Flow-stress anisotropy in aluminum, Acta Metall. Mater. 38 (1990) 1369–1380.
[42] O. Engler, Texture and anisotropy in cold rolled and recovery annealed AA 5182 sheets, Mater. Sci. Technol. 31 (2014) 1058–1065.
[43] Z.Y. Ma, Friction stir processing technology: a review, Metall. Mater. Trans. 39 (2008) 642–658.
[44] X. Meng, Y. Huang, J. Cao, J. Shen, J.F. dos Santos, Recent progress on control strategies for inherent issues in friction stir welding, Prog. Mater. Sci. 115 (2021) 100706.
[45] A. Mishra, B. Kad, F. Gregori, M. Meyers, Microstructural evolution in copper subjected to severe plastic deformation: experiments and analysis, Acta Mater. 55 (2007) 13–28.
[46] F. Tang, J.M. Schoenung, Strain softening in nanocrystalline or ultrafine-grained metals: a mechanistic explanation, Mater. Sci. Eng., A 493 (2008) 101–103.
[47] Y.J. Li, X.H. Zeng, W. Blum, Transition from strengthening to softening by grain boundaries in ultrafine-grained Cu, Acta Mater. 52 (2004) 5009–5018.
[48] R. Kapoor, J.B. Singh, J.K. Chakravartty, High strain rate behavior of ultrafine-grained Al-1.5 Mg, Mater. Sci. Eng., A 496 (2008) 308–315.
[49] N. Kumar, R.S. Mishra, C.S. Huskamp, K.K. Sankaran, Critical grain size for change in deformation behavior in ultrafine grained Al-Mg-Sc alloy, Scripta Mater. 64 (2011) 576–579.
[50] H. Mughrabi, On the grain-size dependence of metal fatigue: outlook on the fatigue of ultrafine-grained metals, Investigations and Applications of Severe Plastic Deformation 80 (2000) 241–253.
[51] C.Y. Yu, P.W. Kao, C.P. Chang, Transition of tensile deformation behaviors in ultrafine-grained aluminum, Acta Mater. 53 (2005) 4019–4028.
[52] N. Kamikawa, T. Hirochi, T. Furuhara, Strengthening mechanisms in ultrafine-grained and sub-grained high-purity aluminum, Metall. Mater. Trans. 50 (2019) 234–248.
[53] Y.S. Sato, M. Urata, H. Kokawa, K. Ikeda, Hall-Petch relationship in friction stir welds of equal channel angular-pressed aluminium alloys, Mater. Sci. Eng., A 354 (2003) 298–305.
[54] V. Bata, E.V. Pereloma, An alternative physical explanation of the Hall-Petch relation, Acta Mater. 52 (2004) 657–665.
[55] P.L. Sun, C.Y. Yu, P.W. Kao, C.P. Chang, Influence of boundary characters on the tensile behavior of sub-micron-grained aluminum, Scripta Mater. 52 (2005) 265–269.
[56] Y.Z. Tian, Y.P. Ren, S. Gao, R.X. Zheng, J.H. Wang, H.C. Pan, Z.F. Zhang, N. Tsuji, G.W. Qin, Two-stage Hall-Petch relationship in Cu with recrystallized structure, J. Mater. Sci. Technol. 48 (2020) 31–35.
[57] Y.S. Sato, M. Urata, H. Kokawa, K. Ikeda, Hall-Petch relationship in friction stir welds of equal channel angular-pressed aluminium alloys, Mater. Sci. Eng., A 354 (2003) 298–305.
[58] X.X. Huang, N. Hansen, N. Tsuji, Hardening by annealing and softening by deformation in nanostructured metals, Science 312 (2006) 249–251.